Open Ceramics 8 (2021) 100197

Contents lists available at ScienceDirect

Open Ceramics

journal homepage: www.sciencedirect.com/journal/open-ceramics

High photocatalytic efficiency of inkjet printed patterns by formulation of eco-friendly TiO_2-based inks

J. Yus [a,b,*], Z. Gonzalez [a,c], A.J. Sanchez-Herencia [a], A. Sangiorgi [d], A. Sanson [d], C. Galassi [d,e], B. Ferrari [a]

[a] Instituto de Cerámica y Vidrio, CSIC, Madrid, Spain
[b] University of Illinois, UIUC, Urbana-Champaign, Illinois, USA
[c] Universidad de Córdoba, UCO, Córdoba, Spain
[d] Institute of Science and Technology for Ceramics, ISTEC-CNR, Faenza, Italy
[e] Department of Mechanical Engineering Politecnico di Milano, Milan Italy

ARTICLE INFO

Keywords:
Inkjet printing
Additive manufacturing
Titanium oxide

ABSTRACT

High photocatalytic performances of inkjet printed patterns has been achieved by a green formulation of water-based suspension including commercial TiO_2 nanoparticles (NPs). The reaction rate constant ($k > 3.79 \times 10-3min-1cm-2$) of the manufactured patterns presented competitive photoresponses in comparison with others complex formulations based on sol-gel process. Optimized conditions of the colloidal dispersion and stabilization of TiO 2 NPs using diethylene glycol as cosolvent, allowed a constant and homogeneous jetting flow, fitting the surface tension and viscosity values suitable for the piezo-driven technology selected. The nanostructure-based pattern printed with micro-resolution achieved the 90% methyl orange degradation after 9h of light exposition and the 100% after 13h in a stirred tank reactor. Moreover, the reusability of printed patterns has been also proved since they preserve their photocatalytic activity and microstructure after sequential tests.

This new finding is expected to be particularly useful to industrial fabrication of microdesign and immobilized patters onto different substrates-types.

1. Introduction

Researchers are spending a lot of effort nowadays to find eco-friendly alternative technologies to tackle environmental issues in many areas of daily life. In smart cities, the removal of pollutants represents a major challenge that has been addressed by defining and monitoring air and water quality parameters and thus adopting solutions to reduce pollutant concentrations. In this sense, introducing functionalities to the typical structural materials that we find in the cities like traffic signs, windows or building facades represents a very interesting opportunity.

The use of semiconductor-assisted photocatalysis for water and air pollutants degradation such as one based on titanium dioxide, TiO_2, is a well-established technology [1]. The use of TiO_2-like catalysts is a method in one of the Advanced Oxidation Processes (AOP) employed in water purification with H_2O_2, UV light and ozone. TiO_2 photocatalysts are an efficient approach for organic molecules degradation. Organic dyes, pesticides, cosmetics, etc., are attacked by the generated OH^- radicals until the complete degradation of the organic matter evolves in an efficient and eco-friendly way.

TiO_2, in the anatase form, is the most frequently used photocatalyst in water purification processes [2] for its properties like relatively low cost and toxicity, water insolubility, and chemical stability. It is commonly used as suspended powder in contaminated water that must be separated after the purification, increasing the complexity of the whole process. To avoid this relevant technological hurdle, several solutions have been proposed [3]. The immobilization of the semiconductor on a substrate is one of the most promising for the photocatalytic removal of organic and inorganic pollutants in water [4] and air [5].

There are many strategies to immobilize catalytic particles onto different and selective substrates depending on the final application of the material. Electrospinning [6,7], film casting [8], chemical vapour deposition [9,10], slip casting or dip-coating [11–13] have been successfully investigated to immobilize TiO_2 on soft and rigid substrates for their use as films, membranes or filters. As an alternative to these conventional methodologies, Additive Manufacturing (AM) techniques

* Corresponding author. Instituto de Cerámica y Vidrio, CSIC, Madrid, Spain.
E-mail addresses: jyus@illinois.edu, joaquinluis.yus@icv.csic.es (J. Yus).

https://doi.org/10.1016/j.oceram.2021.100197
Received 26 August 2021; Received in revised form 1 November 2021; Accepted 3 November 2021
Available online 11 November 2021

have been proven very promising to immobilize the photocatalyst materials and fabricate functional filters [14–17]. Among these rapid prototyping technologies, inkjet printing (IJP) is a well-established route for the fabrication of metal oxide patterns [18,19]. IJP is based on suspensions/inks deposition on a substrate employing a 2D or 3D modelling software for pattering design. An exhaustive control over deposited material amount, the high patterns design precision and the zero-waste process, are some of the advantages of this technique. IJP is also considered a cost-effective processing technique, industrially adapted for mass production of customized products. The viscosity of inkjet inks is normally non-Newtonian and formulations must be adapted/optimized combining different organic solvents and additives to fit the printer requirements [20–22]. The selection of the chemicals that provide the inks with ideal properties is relevant for a successful process. However, due to several environmental factors, nowadays there is a tendency to substitute organic inks by aqueous ones [23]. The use of co-solvents helps to change the evaporation rate of solvent mix and provides proper values of surface tension and viscosity [24]. In particular, glycol as water co-solvent is widely employed in the literature [24,25], as it minimizes drying at the printer nozzles [26], and provides the adequate value of surface tension, viscosity, etc.

The fabrication of well-defined TiO_2 patterns helps to improve the specific active surface of the prints, leading to better photocatalytic and photovoltaic yields thanks to an increase in the number of hydroxyl groups, which triggers the degradation of the organic molecules, and reduces charge recombination phenomena. Innovative TiO_2-based functional inks have been formulated [27,28], either prepared by direct synthesis, (using a sol gel ink deposited onto the substrate and then hydrolized to obtain the TiO_2 solid from the as-printed sol gel ink [29–36]), by dispersing as-synthetized nanopowders in an appropriate medium [26,37–39] or using commercial particles or pastes [40,41] to formulate functional inks.

Among all the cited articles, those that studied the photocatalytic activity of their conformal materials are very interesting. Data related to TiO_2 immobilized coatings and patterns as well as their photocatalytic performance have been recollected in Table 1. Rodriguez et al. [11] measured the N-diethyl-*m*-toluamide (DEET) degradation using a photoreactor in recirculation. Commercial TiO_2 particles were suspended in EtOH and then the substrate, a cylindrical foam (3 cm of diameter and 2.2 cm height), was dip coated and thermally treated at 500 °C. The rapid photocatalytic degradation kinetic was 0.24 min^{-1} when the ozonation occurred simultaneously with the photocatalysis process. Castro et al. synthetized Ca-doped mesoporous TiO_2 NPs by sol-gel to dip coat glass substrates, showing high values of degradation (0.0118 min^{-1}) due to the mesoporosity of the synthetized NPs [42]. In the case of Gonzalez et al. dip coating was also employed to prepare TiO_2 P25 coatings of 1 cm^2 displaying 0.455 h^{-1} degradation of methyl orange (MO). The reactor was a static tank under magnetic stirrer [13]. Moreover, Sangiorgi et al. have performed the degradation analysis in this configuration. They immobilized the TiO_2 P25 particles in a polymeric matrix PLA developing filters by 3D printing obtaining values of kinetics degradation up to 0.0246 h^{-1} [17].

In the field of inkjet some researchers work with liquid sol gel inks and gelled the printed patterns after deposition such as Cerna et al. which deposited a TiO_2 precursor ink on Soda–lime glass plates (25 cm^2). To study the degradation of 2,6-dichloroindophenol (DCIP) they used a flow reactor degrading the organic dye at a reaction rate constant (k) of 1.85×10^{-8} min^{-1} [31]. Kralova et al. also printed a sol-gel ink. They used an Fe and Ag doped TiO_2 precursor with to print substrates of 30 mm × 30 mm displaying a normalized k value of 0.0014 $s^{-1}mol^{-1}cm^2$ after a TT of 450 °C [33]. Moreover, Arin et al. achieved kinetics values in the range of 3.01–4.7 $\times 10^{-4}$ min^{-1} for 4 cm^2 depositions treated at different temperatures (500–650 °C) previously gelled [34]. In another work, they achieved a higher value of k (9.1–11.6 $\times 10^{-4}$ min^{-1}) by mixing the sol gel solution precursor with ethylene glycol (10/1 v/v) to print the same area [20].

Other researchers have used suspensions for the ink formulations. Maleki et al. have synthetized TiO_2 NPs by sol-gel and then suspended in pure ethylene glycol. Photocatalytic activity of the printed samples (40 cm^2) were tested using a flow microreactor and a diluted aqueous solution of methylene blue (MB) (4 ppm) obtaining kinetic constant values between 0.021 and 0.028 min^{-1} [37]. In a similar way, Cerna et al. suspended TiO_2 NPs hydrothermally synthetized into a mixture of water and surfactant solution. Then the ink was printed onto 25 cm^2 and after the TT (500 °C) the fits of kinetic curves show a maximum k value of 0.0313 min^{-1} [32] depending on the employed surfactant.

The printable TiO_2 -based inks reported up today were prepared by complex and long-term procedures, and the semiconductor stabilization in aqueous media was not completely optimized. In our work, commercial TiO_2 NPs were employed to obtain an aqueous ink, which was used to fabricate miniaturized ceramic photo-catalyst coatings. The suspension was formulated to optimize viscosity, surface tension and particle size parameters. Moreover, electric printer parameters such as voltage, pulse, frequency were also adjusted to achieve homogeneous and highly accurate pattern depositions. Microstructural analysis of printed patterns onto FTO-glass were performed by electron microscopy. The consolidation of the nanostructure of the optimized designs were performed by a sintering process at 450 °C. Finally, samples were tested to analyze the photochemical behavior of the printed patterns.

Table 1
Overview of the photocatalytic performance of other similar TiO_2 based photocatalyst.

Ref	TiO_2 nature	Phases/ Composite	Immobilization Processing	Solvent	k values	Photoactive material quantity	Normalized k values (h^{-1} cm^{-2})
[13]	Commercial	TiO_2 P25	Dip coating	H_2O	0.340–0.455 h^{-1}	2.5 g in 1 cm^2	0.340–0.455
[11]	Commercial P25	TiO_2 P25	Dip coating	EtOH	0.005–0.24 min^{-1} Ozonation assisted	30 mm ø x 22 mm thick	0.045–2.182
[42]	Sol gel	TiO_2 Ca doped	Dip coating	Sol gel	0.0068–0.0118 min^{-1}	~70 cm2–335 nm thick	0.006–0.010
[17]	Commercial	PLA/TiO_2 P25	3D printing	–	0.0246 h^{-1}	–	–
[31]	Sol gel	TiO_2	Inkjet	Sol gel	0.89–1.85 $\times 10^{-8}$ min^{-1}	25 cm^2	2.13–4.44 $\times 10^{-8}$
[33]	Sol gel	Ag and Fe doped TiO_2	Inkjet	Sol gel	0.0014 $s^{-1}mol^{-1}cm^2$	9 cm^2	5.04
[34]	Sol gel	TiO_2	Inkjet	Sol gel	3.01–4.7 $\times 10^{-4}$ min^{-1}	4 cm^2	45.15–70.5 $\times 10^{-4}$
[20]	Sol gel	TiO_2	Inkjet	Sol gel and glycols	11.6 $\times 10^{-4}$ min^{-1}	4 cm^2 130–160 nm thick	174 $\times 10^{-4}$
[37]	Sol-gel and Commercial	TiO_2	Inkjet	Ethylene Glycol	0.021–0.028 min^{-1}	~40 cm^2	0.0315–0.042
[32]	Hydrothermal	TiO_2	Inkjet	Water/surfactant (1/1 v/v)	0.0313 min^{-1}	25 cm^2	0.07512

2. Materials and methods

2.1. Ink formulation

All chemicals were of reagent grade and employed without any further purification. The commercial TiO_2 nanopowder (Aeroxide P25, Evonik Degussa GmbH, Germany) used for the ink formulations exhibits a density of 4.2 g/cm^3, a specific surface area (SSA) of 50 ± 15 m^2/g and an anatase:rutile ratio of 80:20.

The as-received TiO_2 NPs was dispersed in a mixture of water and diethylene glycol (DEG). DEG was considered as co-solvent to adjust inks printability and reduce print defects after drying. In order to disperse the TiO_2 NPs, 6 wt% (referred to powder) of a branched polyethylenimine (PEI, pKa 8.6, Mw 25,000 mol/g, Aldrich, Germany) was added and the suspension pH was fixed at 8 using diluted ammonium hydroxide (NH_3) and nitric acid (HNO_3). The as-obtained suspensions of PEI-modified TiO_2 NPs were ball-milled (using Al_2O_3 and ZrO_2 balls of 1 and 0.3 cm in diameter, respectively) in order to break down agglomerates and homogenize the ink. This step of the formulation process was optimized considering different milling times. Aliquots of these suspensions were diluted down to 0.1 g/l in 1:1 DEG:H2O (v/v) at pH 10 to determine their zeta potential and the particle size distribution using a Zetasizer Nano ZS (Malvern Instruments Ltd., Malvern, UK) [43–45]. Using the same instrument, the milling step of the process was studied from 2 up to 48 h aiming at optimizing the particles size. Prior to analysis, the ink was filtered using 1.2 and 0.8 μm Minisart® filters to prevent large particles from reaching the ink tank which could clog the nozzle. The size of the particles must be 50 times lower than the nozzle diameter to avoid clogging [46].

2.2. Ink characterization

The rheology of the solvents mixture was studied as well as the as-prepared inks to properly adjust their viscosity to the printer requirements. Two different equipment were employed. A Haake Mars rheometer (Thermo Scientific, Germany) with a double-cone plate fix of 60 mm of diameter and an angle of 2° (DC60/2°) was used to determine the proper solvent ratio and solid content among suspension with TiO_2 ranging from 15 to 40 wt%. Tests were performed in a control rate mode (CR) from 0 to 1000 s^{-1} in 2 min, dwelling at 1000 s^{-1} for 1 min and shearing down to 0 s^{-1} in 2 min. In control stress mode (CS) the stress was increased from 0 to 15 Pa in 2 min and decreased to 0 Pa in the same time frame. All these tests were done at a constant temperature of 23 ± 0.5 °C. Moreover, in order to study the viscosity at different temperatures (the printer's nozzle can be heated up) a Bohlin C-VOR viscometer (Malvern Instruments) has employed, using a coaxial cylinders (C25) configuration. with bob of 25 mm of diameter and gap 1.25 mm (the height of the bob is 37.5 mm). These analyses were performed with a pre-shear in a control rate mode (CR) from 0 to 1000 s^{-1} in 2 min, dwelling at 1000 s^{-1} for 2 min and shearing down to 0 s^{-1} with the same time. Down-ramps were plotted to study the rheological behavior of the inks.

The average values of surface tension at ambient conditions of the TiO_2-based inks were measured 5 separate times each using a Drop Shape Analyzer – DSA30 Tensiometer (Krüss) in pendant drop configuration. Low values of surface tension are able to promote Newtonian behaviors [14]. Finally, the densities of the suspensions were determined by measuring, for 5 times, the mass of 10 ml of suspension with a graduate test tube and a microbalance.

Then these key physical parameters (viscosity, surface tension, density) used to optimize the jetting and deposition are tied by the Z parameter which is the inverse of the Ohnesorge number. This number is used to predict a successful liquid ejection and it is defined by the equation:

$$Z = \frac{1}{Oh} = \frac{Re}{\sqrt{We}} = \frac{\sqrt{\gamma \rho a}}{\eta} \quad (1)$$

where *Oh* is the Ohnesorge number, *Re* is the Reynolds number and *We* is the Weber number. γ *(N·m)*, η (mPa·s) and ρ (g/cm^3) are the surface tension, the viscosity and the density of the ink, respectively, and *a* (nm) is the nozzle diameter. The optimal range should be $1<Z<10$ [47,48].

2.3. Characterization of prepared layers

Cleaned FTO (Fluorine-doped Tin Oxide)-glasses were used as substrates. Several acetone and ethanol washes in an ultrasonic bath (15 s) were performed for the cleaning. The TiO_2 ink was then printed directly onto the surface forming different patterns on 1 cm^2 area. An XCEL working station (AUREL Automation, Italy) equipped with a piezo-driven inkjet printing head (MD-K-140, Microdrop, Germany) was employed to print the ceramic ink. The main print head characteristics are: 70 μm nozzle diameter, ink tank of 5 ml without recirculation system and 0.4–100 mPa s viscosity range. Briefly, in this equipment drops are ejected by pressure pulse in a fluid filled chamber behind the printing orifice. In a piezoelectric printer this is chiefly controlled by the magnitude of the applied voltage, the actuating pulse duration and its frequency [49,50]. Moreover, the holding pressure in the tank and the temperature of the substrate plate (heated bed) were adjusted. The optimized inkjet-printed TiO_2 patterns were then dried during 15 min on a heating plate at 70 °C and sintered at 450 °C for 15 min and their topography, uniformity and surface morphology characterized by an optical profiler (ZETA, Zeta3D™) and FE-SEM (Hitachi S-4700, Japan).

2.4. Photocatalysis

The photocatalytic behavior of the IJP prints was analyzed following the degradation kinetics of an aqueous dissolution of methyl orange (MO) [17]. The employed light source (Oriel, model 96000) is equipped with a solar light simulating Xe-arc lamp (Osram XBO 450 W). These tests were performed using 25 ml of MO aqueous solution with a concentration of 3.7 mg/l. The pH of the solution was adjusted to 2 using diluted HCl. Photocatalytic measurements were performed introducing the TiO_2 sample in the MO solution that was maintained under continuous irradiation and stirring and capped. Degradation phenomena were monitored using a home-made system described previously elsewhere [17,42]. A narrow band pass filter centered at 500 nm and bandwidth of 10 nm (Thorlabs, FB-500-10 full width at half maximum) was placed in front of a biased Silicon Photodetector (Thorlabs DET100A). The filter allows the light transmission in a wavelength range that matches the absorption band of MO (508 nm). Therefore, the intensity of light at the detector allows measuring the degradation of MO. All the elements were both installed on an optical table to ensure stability and, optically isolated in dark to avoid the presence of other light sources. The output signal from the detector (voltage) was sent to a Keithley 2010 multimeter where it was recorded every 10 min using a Visual Basic home-made code. All measurements were carried out at room temperature.

3. Results and discussion

3.1. TiO_2 ink

The chemical and colloidal stabilization of TiO_2 NPs in aqueous solution was previously tuned [51,52] by the PEI adsorption and estimated from the study of the zeta potential evolution with the pH. The isoelectric point was estimated to be at pH 6–7 and the maximum stability was found from pH 8 where suspensions achieved a zeta potential equal to −30 mV. At pH 8.5, the adsorption of 6 wt% of PEI changes the zeta potential to 50 mV improving the stability of the ink by exploiting both the steric and electrostatic contributions to the stabilization mechanism

[17]. Fig. 1a schematizes the protocol of suspension preparation. Complementary ball-milling studies were carried out to reduce the number of agglomerates (as the scheme of Fig. 1a illustrates) and particle size analyses were performed before printing using dynamic light scattering (DLS). Fig. 1b shows a bi-modal particle size distribution, indicating that some aggregates were not dispersed. However, after 48 h of milling, the volume size distribution changes into a mono-modal feature and the aggregates corresponding to the second peak, with a mean size of 300 nm, disappear. DLS analysis shows that after milling, the TiO_2 particle size is below than 100 nm, smaller than the minimum required for the ink jet printing head considered, which is 1400 nm (~50 times smaller than the nozzle diameter [53]). Then, a 48 h milling was selected. Additionally, the ink was filtered in three sequential stages with membrane filters of 5, 1.2 and 0.8 μm pore size to completely assure the absence of undesired big agglomerates.

The suspension parameters, surface tension, viscosity and solid content, were optimized to favor jetting. PEI stabilized TiO_2 suspensions with 40 wt% of solid content were prepared in the co-solvent H_2O:DEG using different ratios (1:0, 7:3 and 1:1 v/v). Fig. 2a shows the flow curves of as-milled TiO_2 suspensions determined using a double-cone plate tool. All suspensions exhibit thickening behavior. The higher the volume of DEG in the solvent, the more viscous the suspensions. The table at the inset summarizes the surface tension values of these suspensions. While the incorporation of the organic co-solvent lowers the surface tension, the viscosity of the suspension increases. An ink to solvent ratio of (1:1) H_2O:DEG was considered for further studies to prioritize the high water content and the lowest surface tension value. In this sense, once the surface tension (33 ± 4 mN/m) and the TiO_2 NPs dispersion (D_{50} < 100 nm) were optimized, the solid content was adjusted to optimize the flux behavior and prevent settling during printing.

Fig. 2b shows the flow curves for the TiO_2 NPs suspensions with solid loading of 15, 20, 30 and 40 wt% in (1:1 v/v) H_2O:DEG solvent. As expected, the decrease in solid content actually decreased the suspension viscosity. The pseudoplastic behavior of the 40 wt% ink evolves to the quasi-Newtonian flow of the 30 wt% ink, and to the Newtonian response at 20 and 15 wt% solid content. Since the concentration of NPs determines the packing degree of the deposited photoactive material, a solids content of 20 wt% was considered assuming a viscosity of 10 mPa-s with Newtonian behavior leading in a continuous and well controlled ink flow.

The MD-K-140 printing head can be heated to favor the jetting of highly viscous inks, consequently a further rheological characterization was performed as a function of temperature. Fig. 2c illustrates how the temperature modifies the ink flow behavior. The 20 wt% PEI-modified TiO_2 NPs suspension in (1:1 v/v) H_2O:DEG solvent was tested at 25, 35, 45 and 55 °C with a coaxial cylinders geometry. The solvent viscosity was determined at 25 °C as reference.

Predictably, the ink viscosity tends to decrease when the temperature increases. Viscosities are constant along the whole range of shear rate considered, indicating the high stability of the formulated inks. It is important to note that at very high shear rate, the inertia of the suspensions leads to a strong rise in viscosity values due to the geometry (coaxial cylinders) used for the analysis, and should be neglected. Assuming viscosity values showed in Fig. 2c, the selected ink formulation for the print test (20 wt% of solid content dispersed in (1:1 v/v)H_2O:DEG) shows a stable viscosity of about 25–10 mPa s over the whole range of the shear rate, for printing in a temperature range of 25–55 °C.

The Z number was calculated using equation (1), to verify the applicability of this TiO_2 based formulation. Considering the viscosity rage of 25–10 mPa s, the average value of surface tension was 39 ± 1 mNm^{-1} and the density of the suspension was 1.25 g cm^{-3}, the Z parameter was found to be equal to 2.3–5.8, within the ideal printable range [47,48].

In addition to fulfil the Z parameter, the processing conditions, which relate the ink dispersion and stabilization with the printing parameters, should be considered to ensure continuous jet during printing. Fig. 3a shows the MD-K-140 print head, which is provided with a tight reservoir (without recirculation) to store the ink. In this tank, optimized ink stability avoids TiO_2 NPs settling. Moreover, the 70 μm nozzle diameter limits the particle size of TiO_2 in suspension. In this sense, Fig. 3b shows the micrograph of TiO_2 NPs and a detail of the head nozzle at the inset, while Fig. 1c evidences that the full particle population in suspension is below 1400 nm being a priori able to pass through the

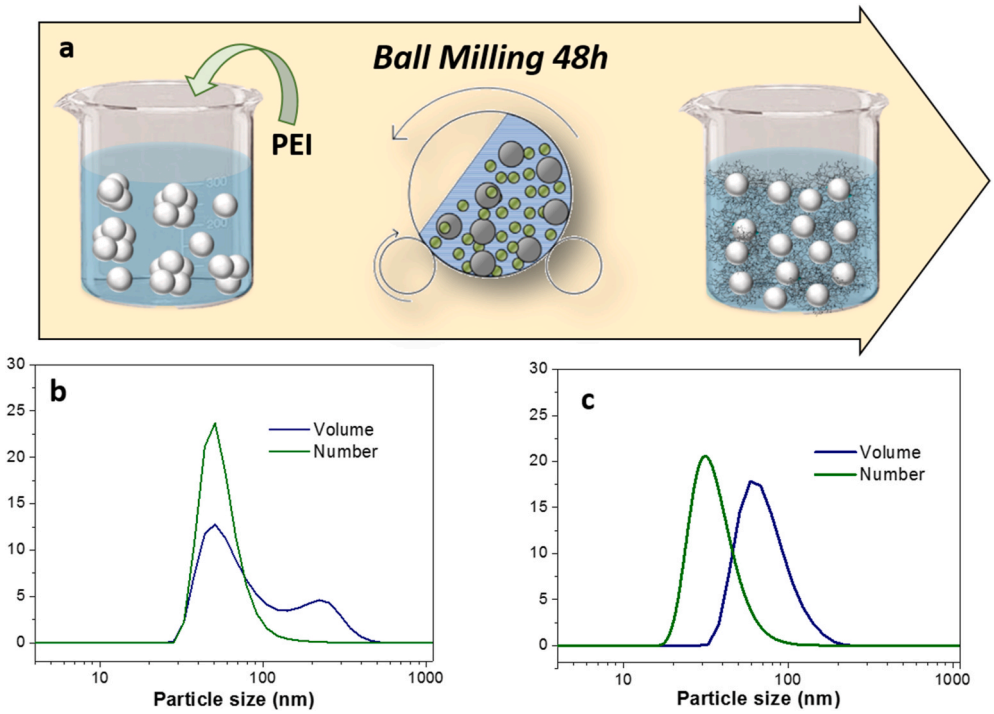

Fig. 1. Scheme of the ink stabilization process (a). Particle size distribution of PEI modified TiO2 NPs dispersed and ball-milled for 1 h (b) and 48 h (c).

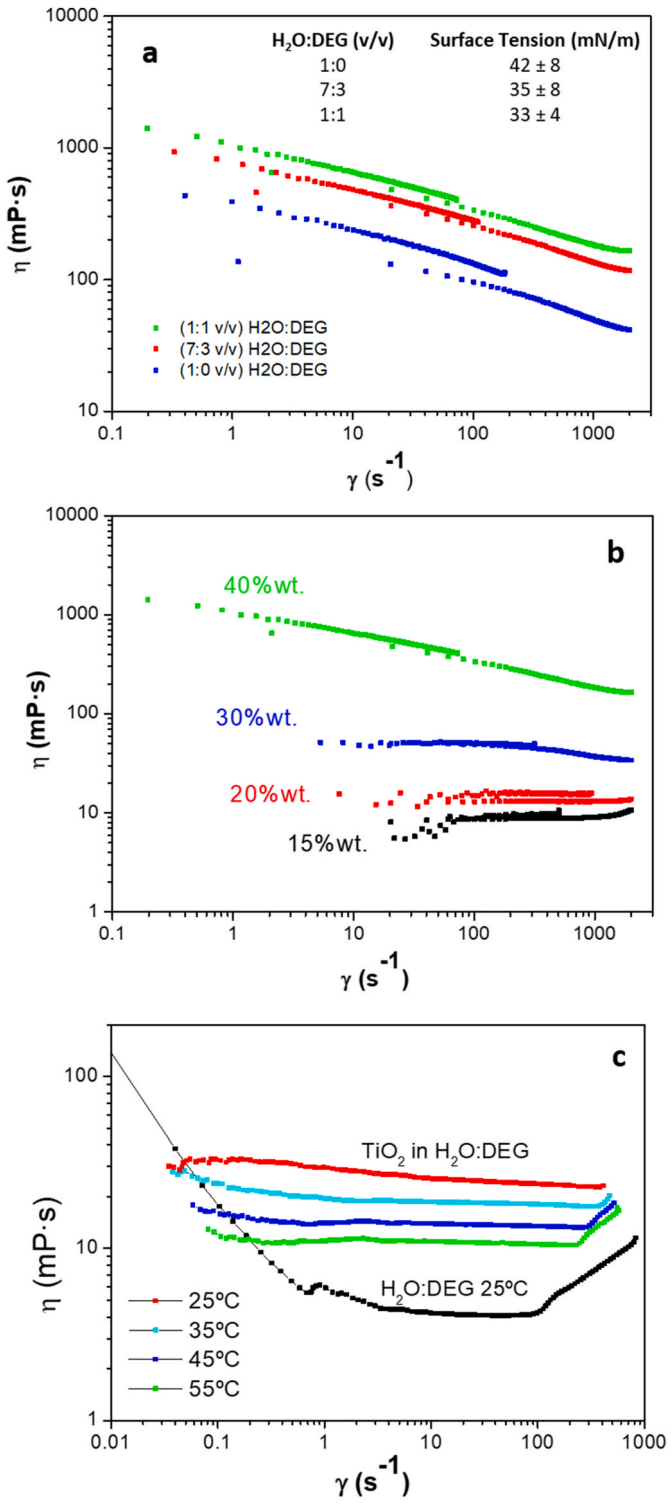

Fig. 2. Flow curves of (a) different ratios of H2O:DEG with 40%wt of solid content, (b) different solid contents with 1:1 ratio of H2O:DEG and (c) different temperatures with a 20%wt of solid content and 1:1 ratio of H2O:DEG.

nozzle. Finally, the viscosity of the ink obtained (Fig. 2) ensures a continuous jet, as shown in the picture in Fig. 3c.

3.2. Characterization of printed patterns

In addition, the optimization of the printing parameters is mandatory to avoid macroscopic and microscopic manufacturing defects, which can deteriorate the structural, microstructural and functional properties of printed patterns. The key process parameters collected in Table 2 guarantee the objective to define reliable printing conditions.

Fig. 4 shows a gallery of printing defects that can appear in TiO_2 patterns, depending on the jetting conditions. Micrograph in Fig. 4a shows a defect of the flow leading to a defect of mass in the pattern, while an excessive jet flow leads to the cracked pattern exhibited in the picture in Fig. 4c. In Fig. 4b, a double jetting due to the partial nozzle closing was detected, and finally the defective pattern in Fig. 4d is the result of the insufficient packing degree that promotes cracking during the drying process.

As evidenced in Fig. 5a, the combination of the ink optimization and the adjusted jetting parameters allowed the printing of uniform TiO_2 patterns without satellite drop spots or crooked drops onto FTO glass. Once the design was specified and the printing optimized, the TiO_2 patterns were sintered and characterized. The thickness (height) and roughness (width) of 1 cm^2 printed grid were determined for one and two layers patterns, and plotted in Fig. 5b. Fig. 5c shows the microscopy image of the grid obtained by printing just one TiO_2 layer. The average height of the prints is 10 μm for one layer and 20 μm for two consecutive printed layers. The printed lines width ranged from 380 to 400 μm, following a uniform pattern. Considering the same figure, the well-known coffee stain effect is slightly perceived just for the thinner pattern (blue line). This phenomenon was explained by Deegan et al. [54], who observed that the solute distribution after the drying was strongly influenced by the solvent evaporation process. However, this effect is suppressed when a second layer is deposited onto the previous one (pink curve).

The FESEM images of the top view of the grids (Fig. 6) reveal a homogeneous and porous microstructure over the whole pattern surface. Low temperature sintering results into macroporosity (<200 μm), that should positively influence the photodegradation ability of printed patterns, since the photoactivity depends on the exposed surface area and the dye accessibility/wettability. In this sense, the 700 μm × 500 μm macroporosity designed by adjusting the grid and the dimensions of the TiO_2 pattern (10/20 μm x 380/400 μm, height x width) provides an exposed area that largely exceeds the geometric surface, considering that the macroporosity of the TiO_2 pattern microstructure also contributes to increasing the area as well as improving the dye wettability. Consequently, both types of porosities will increase the available photocatalytic sites at the illuminated pattern surface during photocatalysis.

3.3. Photocatalytic activity

In order to study the photoactivity of the sintered TiO_2 patterns (0.669 cm^2 total exposed geometrical area) manufactured by IJP, the performance of the sintered coatings was evaluated in terms of MO degradation using a homemade system (Fig. 7a and b). Fig. 7c quantifies the MO photodegradation capability respectively of the two layers and one layer filters. The designed 1-layer grid is able to achieve 90% MO degradation just after 9 h while the thicker grid, composed by two layers, reaches the same result after 15 h. The photoactivity decrease is probably due to a reduction of the residual porosity and consequently of the exposed surface of the pattern due to the percolation of the TiO_2 ink coming from the second layer deposition inside the underlying pores. This result highlights the idea of the larger contribution of the macroporous microstructure of TiO_2 sintered patterns.

Some additional tests were made to study the reusing capability of coatings. Fig. 7d shows the degradation curves during 4 subsequent cycles of 24 h. During the firsts 3 h the degradation remains invariable, then the small deviations between curves are attributed to experimental errors concerning the sample preparation or some irregularities of light intensity in the used equipment. Thus, we could consider that the patterns showed no significant deterioration in photocatalytic performance, which is very important from the application point of view. The good cycling stability highlights the presence of a well-connected

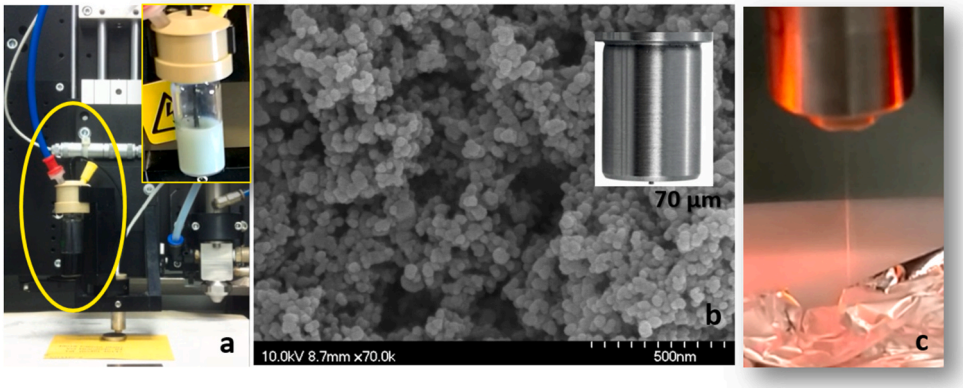

Fig. 3. Pictures of the printer head and the static system for ink storing (a). Electronic microscopy images of the TiO2 NPs (b), and picture of the nozzle and continuous ink jetting (c).

Table 2
Optimized inkjet parameters for the MD-K-140 print head.

Inkjet parameters	Values
Pulse Volt	230 V
Pulse duration	135 us
Frequency	1036 Hz
Strobo Delay	227 us
Holding pressure	−20 mBar
T[a] of the substrate	75 °C
Minimum inter-aligned	50 µm
Motion speed	2.5 cm/s

semiconductor structure as well as a strong adhesion of the TiO_2 layer to the substrate.

Fig. 7e and f, correspond to the kinetic curves of the photocatalytic oxidation of MO fitted by the Langmuir–Hinshelwood model:

$$r = dC/dt = kKC/(1+KC) \quad (2)$$

Where r is the oxidation rate of the reactant, C is the concentration of the reactant, t is the illumination time, k is the reaction rate constant, and K is the adsorption coefficient of the reactant. Because of the low initial concentration of the dye (C0), equation (2) was simplified to a first-order equation:

$$\ln (C0/C) = kt \quad (3)$$

Fig. 7e illustrates the difference in terms of degradation kinetic between layer 1 and 2 of the TiO_2 patterns showing faster reactions when only one layer is deposited because its higher porosity. In Fig. 7f, the number of cycles does not decrease the reaction rate constant. "k" remains almost invariant over the cycles, which shows a very promising cycling capability for use in continuous reactors. The k values are summarized in Table 3.

The photocatalytic degradation performance of the inkjet-printed TiO_2 patterns were similar to that reported for samples, based on the

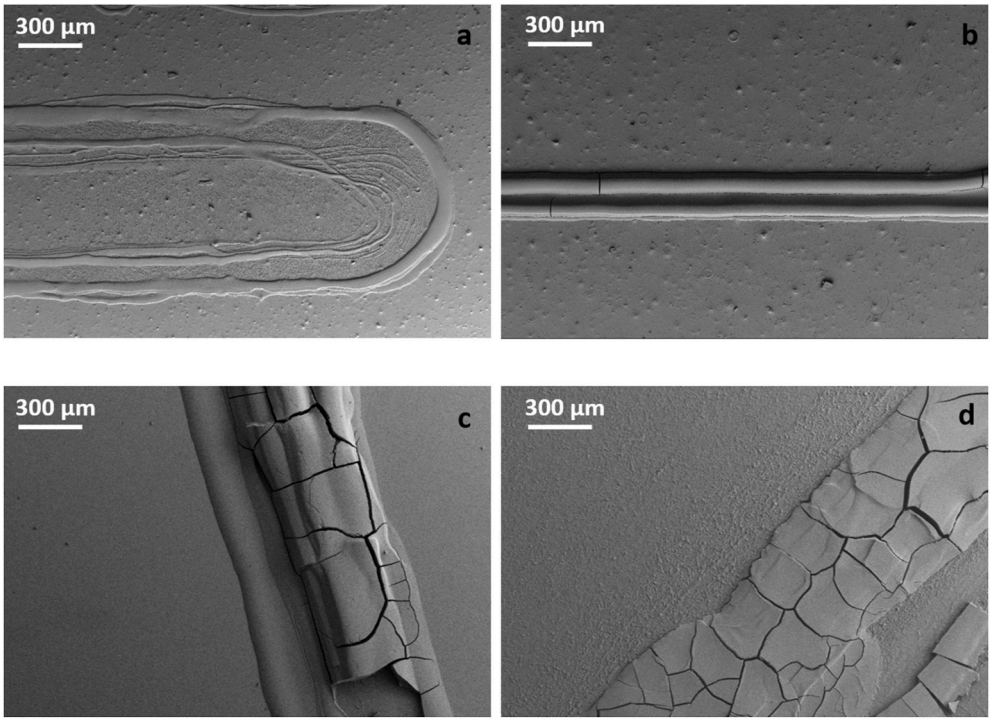

Fig. 4. Electronic microscopy images of the deflected patterns obtained: different height along the pattern (a), double jetting (b), and cracks (c and d).

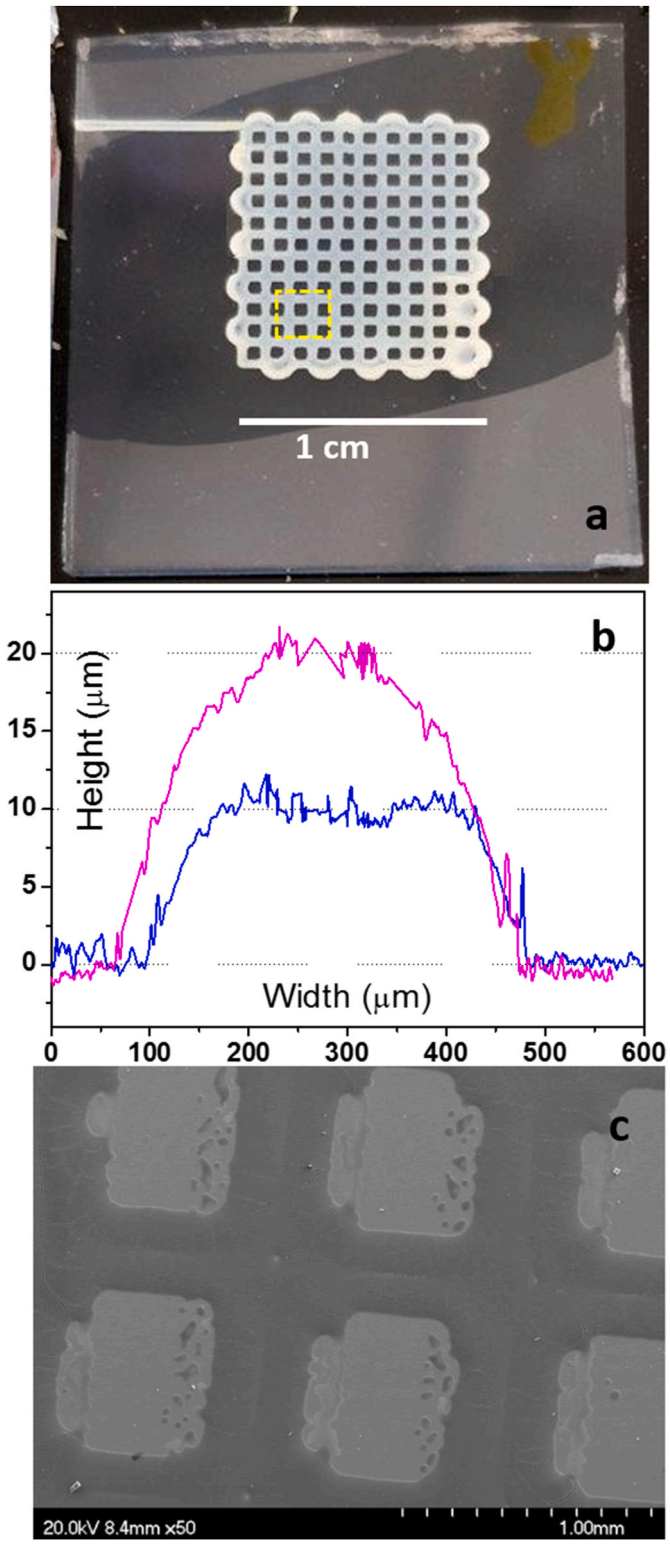

Fig. 5. Picture of one-layer printed and sintered sample (a). Profilometry and height of one and two layers patterns (b). Electronic microscopy images of the top view of one-layer deposited and sintered sample (c).

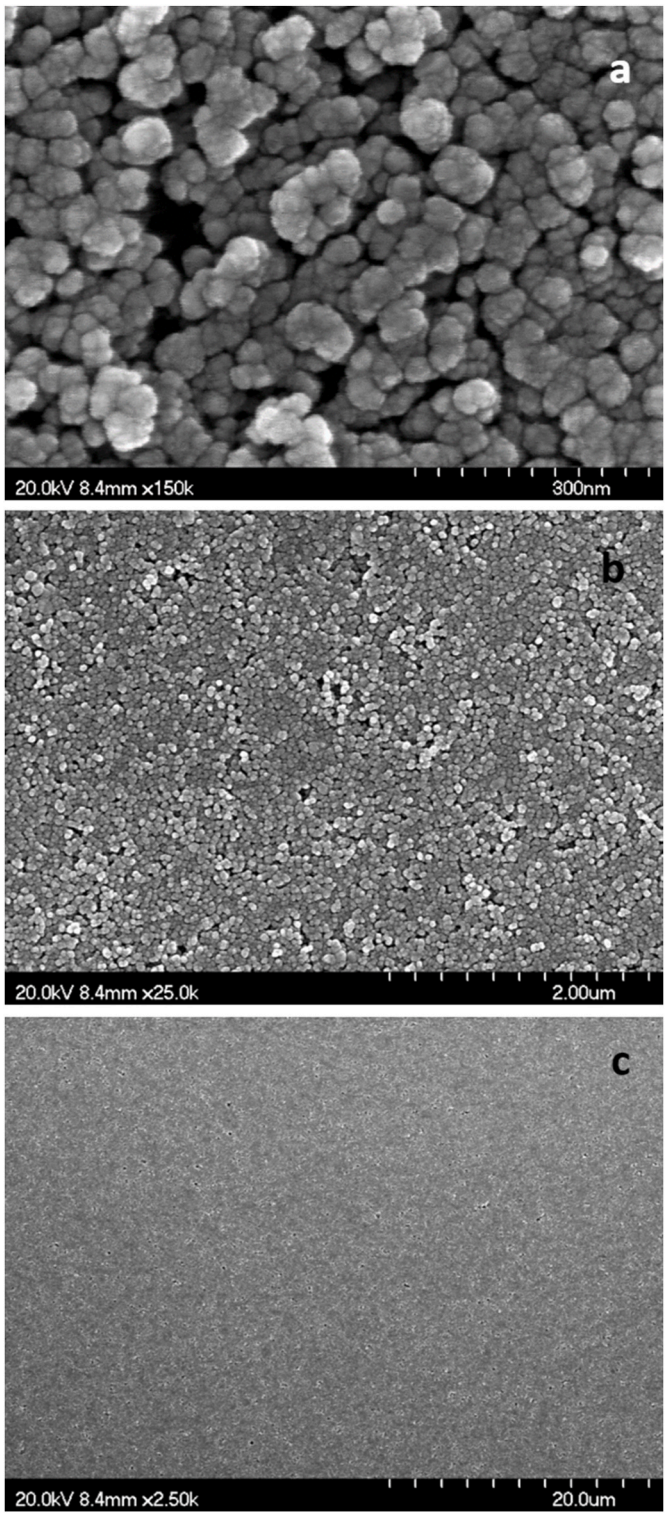

Fig. 6. SEM images of the top view of the 1Layer deposited patterns taken at x 150k (a); x25k (b) and x 2.5k magnification (c).

same semiconductor, prepared by other methods [17,42]. The results reported in this work suggest that the IJP of TiO_2 NPs is a reliable alternative to print patterns with a high resolution with a real normalized kinetic constant up to 3.79×10^{-3} $min^{-1}cm^{-2}$. New patterns of micro-filters could be designed, optimized and printed to increase the exposed surface, providing fast degradation reactions to efficiently depollute water.

4. Conclusions

This study illustrates an innovative design of photoactive TiO_2 microfilters by IJP. The photodegradation tests showed patterns capable to withstand multiple long cycles (24h for 4 times) and short degradation times (3h for 1.85 ppm of MO degradation) comparable to other

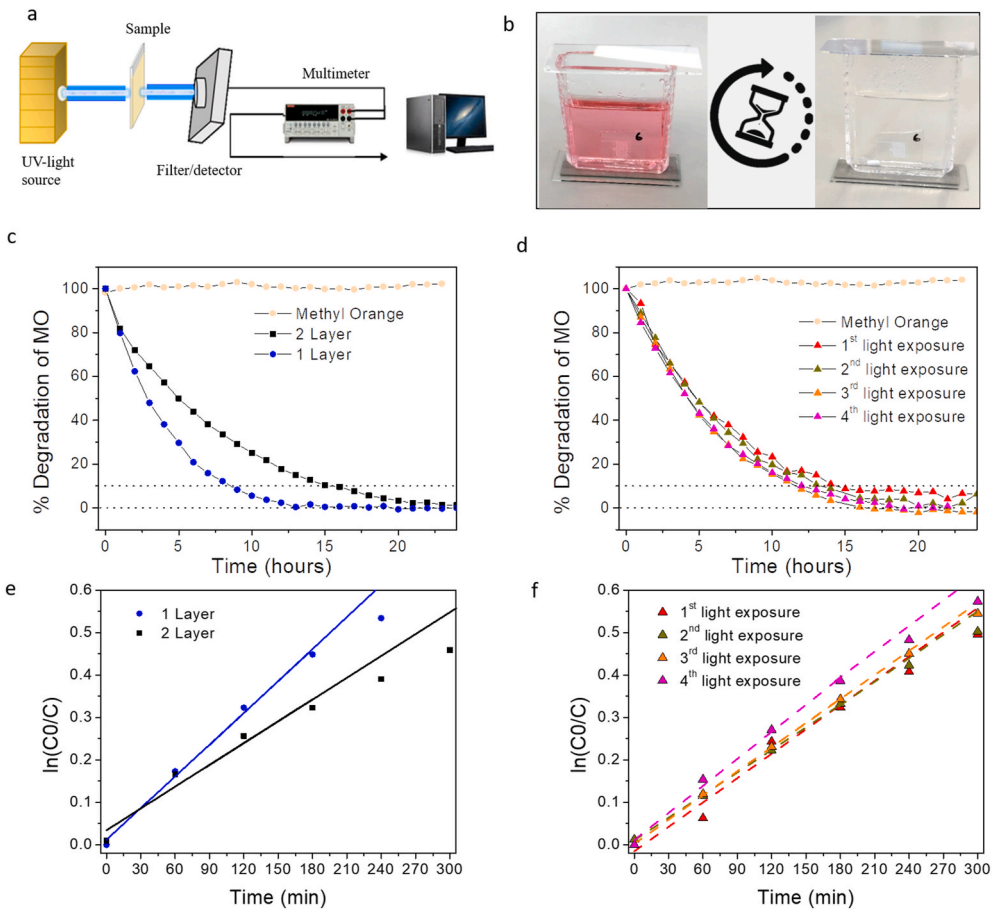

Fig. 7. Scheme of the homemade degradation measurement system (a). Picture of the samples inside the MO solution before and after 24h of UV-light exposure (b). Photodegradation of MO under 24h of light exposure of 1 and 2 layered samples (c) and 4 cycles of light exposure (d). Kinetics of degradation during the 5 first hours for 1 and 2 layers (e) and the cycled sample (f).

Table 3
Degradation kinetics values.

Sample description	TiO_2 mass (mg)	Coating thickness/Pattern height (μm)	Active surface (cm^2 of TiO_2)	k
1 Layer	1.95	10	0.66	0.0025 min^{-1} = 0.149 h^{-1}
2 Layer	~4.0	20	0.66	0.0017 min^{-1} = 0.102 h^{-1}
Cycle 4th of light exposure	0.527	10	0.66	0.0021 min^{-1} = 0.127 h^{-1}

filters fabricated by using traditional technologies. The use of commercial nanoparticles and the easy processing and formulation of the inks facilitate the transference to industry of microfilters that can be printed onto different substrates-types. The reaction rate constant calculated from fitting the kinetic curves shows k values up to 0.0025 min^{-1} and 3.79 × 10^{-3} min^{-1} cm^{-2} with high cycling capability for use in continuous reactors. The amount of deposited mass, raising the number of printed layers induces the partial closing of pores of the firsts TiO_2 layers reducing the residual porosity and the exposed surface thus decreasing the photodegradation capability.

As an additive manufacturing technique, IJP offers numerous advantages for environmental health and safety applications thanks to the reduction of both wastes production and potentially expensive and/or toxic raw nanomaterials. In fact, an environmentally friendly ink for IJP was formulated containing 50% of water, minimizing the use of organics and thus reducing its carbon footprint. The milling process allows achieving particles of maximum 200 nm leading to an ink with long time stability. The use of DEG as co-solvent results in optimal values of viscosity, surface tension and Z-number. The electrical parameters of the piezo-driven printing head were adjusted and optimized in order to obtain a continuous jetting flow of the desired ink, avoiding unnecessary waste of time and material. Furthermore, the nanostructure-based patterns printed with micro-resolution were sintered at low temperature (450 °C, 15 min) to consolidate the macroporosity microstructure, that should positively influence the photodegradation ability of robust printed patterns.

Declaration of competing interest

The authors declare that they have no known competing financial interests or personal relationships that could have appeared to influence the work reported in this paper.

Acknowledgments

The authors thank ECERS grant JECS Trust for funding this project under the contract 2017141. Part of this work was also carried out thanks to the financial support of ADITIMAT-CM (CAM: S2018/NMT-4411) and MicroMatters@AM (PID2019-106631 GB-C42).

References

[1] S. Mills, Andrew, Hunte Le, An Overview of semiconductor photocatalysis, Photochem. Photobiol. 108 (1997) 1–35, https://doi.org/10.1126/science.12.296.346-a.

[2] T. Ochiai, K. Masuko, S. Tago, R. Nakano, K. Nakata, M. Hara, Y. Nojima, T. Suzuki, M. Ikekita, Y. Morito, A. Fujishima, Synergistic water-treatment reactors using a TiO_2-modified Ti-mesh filter, Water (Switzerland) 5 (2013) 1101–1115, https://doi.org/10.3390/w5031101.

[3] A. Sobczyński, A. Dobosz, Water purification by photocatalysis on semiconductors, Pol. J. Environ. Stud. 10 (2001) 195–205.

[4] A.Y. Shan, T.I.M. Ghazi, S.A. Rashid, Immobilisation of titanium dioxide onto supporting materials in heterogeneous photocatalysis: a review, Appl. Catal. Gen. 389 (2010) 1–8, https://doi.org/10.1016/j.apcata.2010.08.053.

[5] A. Talaiekhozani, S. Rezania, K.H. Kim, R. Sanaye, A.M. Amani, Recent advances in photocatalytic removal of organic and inorganic pollutants in air, J. Clean. Prod. 278 (2021) 123895, https://doi.org/10.1016/j.jclepro.2020.123895.

[6] M. Mousakhani, N. Sarlak, Electrospun composite nanofibre adsorbents for effective removal of Cd^{2+} from polluted water, Mater. Chem. Phys. 256 (2020) 123578, https://doi.org/10.1016/j.matchemphys.2020.123578.

[7] H. Rongan, L. Haijuan, L. Huimin, X. Difa, Z. Liuyang, S-scheme photocatalyst Bi_2O_3/TiO_2 nanofiber with improved photocatalytic performance, J. Mater. Sci. Technol. 52 (2020) 145–151, https://doi.org/10.1016/j.jmst.2020.03.027.

[8] F.A. Sabah, I.A. Razak, E.A. Kabaa, M.F. Zaini, A.F. Omar, Characterization of hybrid organic/inorganic semiconductor materials for potential light emitting applications, Opt. Mater. 107 (2020) 110117, https://doi.org/10.1016/j.optmat.2020.110117.

[9] S. Brown, J. Lengaigne, N. Sharifi, M. Pugh, C. Moreau, A. Dolatabadi, L. Martinu, J.E. Klemberg-Sapieha, Durability of superhydrophobic duplex coating systems for aerospace applications, Surf. Coating. Technol. 401 (2020), https://doi.org/10.1016/j.surfcoat.2020.126249.

[10] B. Astinchap, H. Ghanbaripour, R. Amuzgar, Multifractal study of TiO_2 thin films deposited by MO-CVD method: the role of precursor amount and substrate temperature, Optik 222 (2020) 165384, https://doi.org/10.1016/j.ijleo.2020.165384.

[11] E.M. Rodríguez, A. Rey, E. Mena, F.J. Beltrán, Application of solar photocatalytic ozonation in water treatment using supported TiO_2, Appl. Catal. B Environ. 254 (2019) 237–245, https://doi.org/10.1016/j.apcatb.2019.04.095.

[12] J.G. Mahy, C. Wolfs, A. Mertes, C. Vreuls, S. Drot, S. Smeets, S. Dircks, A. Boergers, J. Tuerk, S.D. Lambert, Advanced photocatalytic oxidation processes for micropollutant elimination from municipal and industrial water, J. Environ. Manag. 250 (2019) 109561, https://doi.org/10.1016/j.jenvman.2019.109561.

[13] Z. Gonzalez, J. Yus, Y. Bravo, A.J. Sanchez-herencia, Exploitation of Lignocellulose Fiber-Based Biotemplates to Improve the Performance of an Immobilized TiO_2 Photocatalyst, 2021.

[14] F. Zhang, M. Wei, V.V. Viswanathan, B. Swart, Y. Shao, G. Wu, C. Zhou, 3D printing technologies for electrochemical energy storage, Nanomater. Energy 40 (2017) 418–431, https://doi.org/10.1016/j.nanoen.2017.08.037.

[15] C. Hurt, M. Brandt, S.S. Priya, T. Bhatelia, J. Patel, P.R. Selvakannan, S. Bhargava, Combining additive manufacturing and catalysis: a review, Catal. Sci. Technol. 7 (2017) 3421–3439, https://doi.org/10.1039/c7cy00615b.

[16] C. Parra-Cabrera, C. Achille, S. Kuhn, R. Ameloot, 3D printing in chemical engineering and catalytic technology: structured catalysts, mixers and reactors, Chem. Soc. Rev. 47 (2018) 209–230, https://doi.org/10.1039/c7cs00631d.

[17] A. Sangiorgi, Z. Gonzalez, A. Ferrandez-Montero, J. Yus, A.J. Sanchez-Herencia, C. Galassi, A. Sanson, B. Ferrari, 3D printing of photocatalytic filters using a biopolymer to immobilize TiO_2 nanoparticles, J. Electrochem. Soc. 166 (2019) H3239–H3248, https://doi.org/10.1149/2.0341905jes.

[18] C. Zhu, A.J. Pascall, N. Dudukovic, M.A. Worsley, J.D. Kuntz, E.B. Duoss, C. M. Spadaccini, Colloidal materials for 3D printing, Annu. Rev. Chem. Biomol. Eng. 10 (2019) 17–42, https://doi.org/10.1146/annurev-chembioeng-060718-030133.

[19] B. Derby, Additive manufacture of ceramics components by inkjet printing, Engineering 1 (2015) 113–123, https://doi.org/10.15302/J-ENG-2015014.

[20] M. Arin, P. Lommens, S.C. Hopkins, G. Pollefeyt, J. Van Der Eycken, S. Ricart, X. Granados, B.A. Glowacki, I. Van Driessche, Deposition of photocatalytically active TiO 2 films by inkjet printing of TiO_2 nanoparticle suspensions obtained from microwave-assisted hydrothermal synthesis, Nanotechnology 23 (2012), https://doi.org/10.1088/0957-4484/23/16/165603.

[21] C. Gadea, Q. Hanniet, A. Lesch, D. Marani, S.H. Jensen, V. Esposito, Aqueous metal-organic solutions for YSZ thin film inkjet deposition, J. Mater. Chem. C. 5 (2017) 6021–6029, https://doi.org/10.1039/c7tc01879g.

[22] M. Liu, J. Wang, M. He, L. Wang, F. Li, L. Jiang, Y. Song, Inkjet printing controllable footprint lines by regulating the dynamic wettability of coalescing ink droplets, ACS Appl. Mater. Interfaces 6 (2014) 13344–13348, https://doi.org/10.1021/am5042548.

[23] T. Bakarič, B. Malič, D. Kuscer, Lead-zirconate-titanate-based thick-film structures prepared by piezoelectric inkjet printing of aqueous suspensions, J. Eur. Ceram. Soc. 36 (2016) 4031–4037, https://doi.org/10.1016/j.jeurceramsoc.2016.06.038.

[24] H.H. Lee, K. Sen Chou, K.C. Huang, Inkjet printing of nanosized silver colloids, Nanotechnology 16 (2005) 2436–2441, https://doi.org/10.1088/0957-4484/16/10/074.

[25] D. Pech, M. Brunet, P.L. Taberna, P. Simon, N. Fabre, F. Mesnilgrente, V. Conédéra, H. Durou, Elaboration of a microstructured inkjet-printed carbon electrochemical capacitor, J. Power Sources 195 (2010) 1266–1269, https://doi.org/10.1016/j.jpowsour.2009.08.085.

[26] R. Cherrington, D.J. Hughes, S. Senthilarasu, V. Goodship, Inkjet-printed TiO2 nanoparticles from aqueous solutions for dye-sensitized solar cells (DSSCs), Energy Technol. 3 (2015) 866–870, https://doi.org/10.1002/ente.201500096.

[27] M. Fang, T. Li, S. Zhang, K.V. Rao, L. Belova, Design and tailoring of inks for inkjet patterning of metal oxides, R. Soc. Open Sci. 7 (2020), https://doi.org/10.1098/rsos.200242.

[28] H. Maleki, V. Bertola, Recent advances and prospects of inkjet printing in heterogeneous catalysis, Catal. Sci. Technol. 10 (2020) 3140–3159, https://doi.org/10.1039/d0cy00040j.

[29] B. Bourgeois, S. Luo, B. Riggs, Y. Ji, S. Adireddy, K. Schroder, S. Farnsworth, D. Chrisey, M. Escarra, Pulsed photoinitiated fabrication of inkjet printed titanium dioxide/reduced graphene oxide nanocomposite thin films, Nanotechnology 29 (2018), https://doi.org/10.1088/1361-6528/aac306.

[30] E.P. Simonenko, A.S. Mokrushin, N.P. Simonenko, V.A. Voronov, V.P. Kim, S. V. Tkachev, S.P. Gubin, V.G. Sevastyanov, N.T. Kuznetsov, Ink-jet printing of a TiO_2–10%ZrO_2 thin film for oxygen detection using a solution of metal alkoxoacetylacetonates, Thin Solid Films 670 (2019) 46–53, https://doi.org/10.1016/j.tsf.2018.12.004.

[31] M. Černá, M. Veselý, P. Dzik, Physical and chemical properties of titanium dioxide printed layers, Catal. Today 161 (2011) 97–104, https://doi.org/10.1016/j.cattod.2010.11.019.

[32] M. černá, M. Veselý, P. Dzik, C. Guillard, E. Puzenat, M. Lepičová, Fabrication, characterization and photocatalytic activity of TiO_2 layers prepared by inkjet printing of stabilized nanocrystalline suspensions, Appl. Catal. B Environ. 138–139 (2013) 84–94, https://doi.org/10.1016/j.apcatb.2013.02.035.

[33] M. Kralova, P. Dzik, M. Vesely, J. Cihlar, Preparation and characterization of doped titanium dioxide printed layers, Catal. Today 230 (2014) 188–196, https://doi.org/10.1016/j.cattod.2013.09.018.

[34] M. Arin, P. Lommens, N. Avci, S.C. Hopkins, K. De Buysser, I.M. Arabatzis, I. Fasaki, D. Poelman, I. Van Driessche, Inkjet printing of photocatalytically active TiO_2 thin films from water based precursor solutions, J. Eur. Ceram. Soc. 31 (2011) 1067–1074, https://doi.org/10.1016/j.jeurceramsoc.2010.12.033.

[35] J.S. Gebauer, V. Mackert, S. Ognjanović, M. Winterer, Tailoring metal oxide nanoparticle dispersions for inkjet printing, J. Colloid Interface Sci. 526 (2018) 400–409, https://doi.org/10.1016/j.jcis.2018.05.006.

[36] I.M. Hossain, D. Hudry, F. Mathies, T. Abzieher, S. Moghadamzadeh, D. Rueda-Delgado, F. Schackmar, M. Bruns, R. Andriessen, T. Aernouts, F. Di Giacomo, U. Lemmer, B.S. Richards, U.W. Paetzold, A. Hadipour, Scalable processing of low-temperature TiO_2 nanoparticles for high-efficiency perovskite solar cells, ACS Appl. Energy Mater. 2 (2019) 47–58, https://doi.org/10.1021/acsaem.8b01567.

[37] H. Maleki, V. Bertola, TiO2 nanofilms on polymeric substrates for the photocatalytic degradation of methylene blue, ACS Appl. Nano Mater. 2 (2019) 7237–7244, https://doi.org/10.1021/acsanm.9b01723.

[38] A.M. Barreiro, G.K. Pinheiro, B.N. Wesling, D. Müller, L.T. Scarabelot, L.V. De Souza, D. Hotza, C.R. Rambo, Aerogel-based TiO_2 stable inks for direct inkjet printing of nanostructured layers, Adv. Mater. Sci. Eng. 2020 (2020), https://doi.org/10.1155/2020/4273097.

[39] X. Zhan, C. Yan, Y. Zhang, G. Rinke, G. Rabsch, M. Klumpp, A.I. Schäfer, R. Dittmeyer, Investigation of the reaction kinetics of photocatalytic pollutant degradation under defined conditions with inkjet-printed TiO_2 films-from batch to a novel continuous-flow microreactor, React. Chem. Eng. 5 (2020) 1658–1670, https://doi.org/10.1039/d0re00238k.

[40] A.J. Huckaba, I. Garcia-Benito, H. Kanda, N. Shibayama, E. Oveisi, S. Kinge, M. K. Nazeeruddin, Inkjet-printed TiO_2/fullerene composite films for planar perovskite solar cells, Helv. Chim. Acta 103 (2020), https://doi.org/10.1002/hlca.202000044.

[41] I. Bernacka-Wojcik, P.J.J. Wojcik, H. Aguas, E. Fortunato, R. Martins, Inkjet printed highly porous TiO_2 films for improved electrical properties of photoanode, J. Colloid Interface Sci. 465 (2016) 208–214, https://doi.org/10.1016/j.jcis.2015.11.070.

[42] Y. Castro, A. Durán, Ca doping of mesoporous TiO2 films for enhanced photocatalytic efficiency under solar irradiation, J. Sol. Gel Sci. Technol. 78 (2016) 482–491, https://doi.org/10.1007/s10971-016-3988-1.

[43] Z. Gonzalez, J. Yus, A. Caballero, J. Morales, A.J. Sanchez-Herencia, B. Ferrari, Electrochemical performance of pseudo-capacitor electrodes fabricated by Electrophoretic Deposition inducing $Ni(OH)_2$ nanoplatelets agglomeration by Layer-by-Layer, Electrochim. Acta 247 (2017) 333–343, https://doi.org/10.1016/j.electacta.2017.07.043.

[44] J. Yus, B. Ferrari, A. Sanchez-Herencia, A. Caballero, J. Morales, Z. Gonzalez, In situ synthesis and electrophoretic deposition of NiO/Ni core-shell nanoparticles and its application as pseudocapacitor, Coatings 7 (2017) 193, https://doi.org/10.3390/coatings7110193.

[45] J. Yus, Y. Bravo, A.J. Sanchez-Herencia, B. Ferrari, Z. Gonzalez, Electrophoretic deposition of RGO-NiO core-shell nanostructures driven by heterocoagulation method with high electrochemical performance, Electrochim. Acta 308 (2019) 363–372, https://doi.org/10.1016/j.electacta.2019.04.053.

[46] J.L. Valero, C. Jarom, E. Comas, Optimized Automatic Recovery of Nozzle Health in Inkjet Systems, Program, 2018, pp. 766–770.

[47] P. He, B. Derby, Inkjet printing ultra-large graphene oxide flakes, 2D Mater. 4 (2017), https://doi.org/10.1088/2053-1583/aa629e.

[48] Y.F. Liu, M.H. Tsai, Y.F. Pai, W.S. Hwang, Control of droplet formation by operating waveform for inks with various viscosities in piezoelectric inkjet printing, Appl. Phys. Mater. Sci. Process 111 (2013) 509–516, https://doi.org/10.1007/s00339-013-7569-7.

[49] N. Reis, C. Ainsley, B. Derby, Ink-jet delivery of particle suspensions by piezoelectric droplet ejectors, J. Appl. Phys. 97 (2005), https://doi.org/10.1063/1.1888026.

[50] J. Yus, Z. Gonzalez, A.J.J. Sanchez-Herencia, A. Sangiorgi, N. Sangiorgi, D. Gardini, A. Sanson, C. Galassi, A. Caballero, J. Morales, B. Ferrari, Semiconductor water-based inks: miniaturized NiO pseudocapacitor electrodes by inkjet printing, J. Eur. Ceram. Soc. 39 (2019), https://doi.org/10.1016/j.jeurceramsoc.2019.03.020, 0–1.

[51] Z. Gonzalez, J. Yus, A.J.J. Sanchez-Herencia, J. Dewalque, L. Manceriu, C. Henrist, B. Ferrari, A colloidal approach to prepare binder and crack-free TiO_2 multilayer coatings from particulate suspensions: application in DSSCs, J. Eur. Ceram. Soc. 39 (2019) 366–375, https://doi.org/10.1016/j.jeurceramsoc.2018.09.018.

[52] Z. Gonzalez, J. Yus, Y. Bravo, A.J. Sanchez-Herencia, A. Rodríguez, J. Dewalque, L. Manceriu, C. Henrist, B. Ferrari, Heteroacoagulation of lignocellulose fibers-based biotemplates and functionalized TiO_2 nanoparticles to tailor film microstructures, Cellulose 27 (2020) 7543–7559, https://doi.org/10.1007/s10570-020-03297-1.

[53] P. Sundriyal, S. Bhattacharya, Inkjet-printed electrodes on A4 paper substrates for low-cost, disposable, and flexible asymmetric supercapacitors, ACS Appl. Mater. Interfaces 9 (2017) 38507–38521, https://doi.org/10.1021/acsami.7b11262.

[54] R.D. Deegan, O. Bakajin, T.F. Dupont, G. Huber, S.R. Nagel, T.A. Witten, Capillary flow as the cause of ring stains from dried liquid drops, Nature 389 (1997) 827–829, https://doi.org/10.1038/39827.